Exceptional points by coupling of modes with different angular momenta in deformed microdisks: A perturbative analysis

Julius Kullig,[1,*] Chang-Hwan Yi,[2,1] and Jan Wiersig[1]
[1]*Institut für Physik, Otto-von-Guericke-Universität Magdeburg, Postfach 4120, D-39016 Magdeburg, Germany*
[2]*Department of Emerging Materials Science, DGIST, Daegu 711-873, Korea*

(Received 29 May 2018; published 27 August 2018)

Recently, it has been shown numerically and by a semiclassical approach [Phys. Rev. Lett. **120**, 093902 (2018)] that second-order exceptional points can appear in the spectrum of weakly deformed microdisk resonators by coupling of optical modes with different angular momentum. Here, we use a perturbation theory for weak boundary deformations to derive an effective non-Hermitian Hamiltonian from which we obtain analytical formulas to describe the formation of second-order exceptional points in such systems. The theory is extended to third-order exceptional points and confirmed by full numerical calculations.

DOI: 10.1103/PhysRevA.98.023851

I. INTRODUCTION

The observation of interesting and unconventional physics at and near exceptional points (EPs) in quantum and wave systems with dissipation and/or gain has triggered significant activity in recent years. In contrast with conventional degeneracies at an EP, not only eigenvalues but also the corresponding eigenstates coalesce [1–3]. Various experiments have demonstrated the existence of second-order EPs (EP2s), where exactly two eigenvalues and eigenstates coalesce in physical systems, e.g., in microwave cavities [4,5], optical microcavities [6–9], coupled atom-cavity systems [10], exciton-polariton billiards [11], and acoustic shells [12]. EPs have already found several applications, e.g., as ultrasensitive sensors [13,14], unidirectional lasing operation in microlasers [9], orbital angular-momentum lasers [15], sources of circularly polarized light [16], and for energy transfer between modes [17,18].

Higher-order EPs, involving more than two eigenstates, have been experimentally realized only recently by using coupled acoustic cavities with asymmetric dissipation [19] and in parity-time-symmetric photonic molecules [20]. Interesting new aspects of higher-order EPs include more complex topology [21], a different definition of chirality [22], extreme dynamical behavior [23], and even higher sensitivity [20].

Optical microcavities are essential ingredients of novel light-emitting devices, e.g., single-photon emitters [24], lasers with ultralow threshold [25], and sources of entangled photon pairs [26]. Dissipation is present in the form of material absorption or gain and radiation losses. Important examples of microcavities are whispering-gallery cavities where light is trapped by total internal reflection at the boundary of the cavity. Deforming or perturbing the boundary of such cavities can be beneficial for several applications (see Ref. [27] for a review), e.g., directional free-space light emission [28–32], mode selection [33], and broadband efficient waveguide coupling [34].

In a recent paper of the authors, it was shown that EP2s can be generated in microdisks with extremely weak boundary deformation after fine tuning the refractive index [35]. This surprising effect was explained with a semiclassical theory based on resonance-assisted tunneling in ray-dynamical phase space. The aim of the present paper is to exploit a perturbation theory for weak boundary deformations [36] to get an even deeper understanding of the appearance of EPs in such systems. The perturbation theory allows us to derive explicit formulas for the location of the EPs in parameter space. Moreover, we develop an approach where fine tuning of refractive index is no longer necessary. Finally, we show that our approach can be extended to higher-order EPs, which we demonstrate for an EP of third order (EP3).

This paper is organized as follows: In Sec. II we review the relevant aspects of the perturbation theory. The effective Hamiltonian for two nearly degenerate modes is introduced in Sec. III. This Hamiltonian is used in Sec. IV to find EP2s for general smooth boundaries with a fine-tuned refractive index and in Sec. V for specially designed boundaries without the need of fine tuning the refractive index. In Sec. VI we extend the theory to an EP3. The paper is concluded in Sec. VII.

II. PERTURBATION THEORY FOR TWO NEARLY DEGENERATE MODES

In this section we briefly review the main results of the perturbation theory relevant for the first-order treatment of two nearly degenerate modes in a slightly deformed microdisk cavity [36]. The zeroth-order solutions are the modes in the circular cavity of radius R with complex frequency ω (wave number $k = \omega/c$, where c is the speed of light in vacuum) labeled by the azimuthal (angular momentum) mode number m and the radial mode number l. The dimensionless frequencies $x = \omega R/c = kR$ of these modes for transverse-magnetic (TM) polarization are given by the roots of

$$S_m(x) = n\frac{J_m'}{J_m}(nx) - \frac{H_m'}{H_m}(x). \tag{1}$$

*julius.kullig@ovgu.de

Here, n is the (effective) refractive index, J_m and H_m are the Bessel and Hankel functions of the first kind and of order m. The prime ($'$) denotes the first derivative with respect to the argument of the function.

The theory treats a boundary deformation of the type

$$r(\phi) = R + \lambda f(\phi), \tag{2}$$

with formal perturbation parameter λ which is set to unity at the end. The deformation function $f(\phi)$ is 2π periodic and even with respect to $\phi = 0$, so only boundary deformations with a remaining mirror-reflection symmetry can be studied (see Ref. [37] for more general geometries). The even- and odd-parity modes of the deformed cavity are expanded in the even- and odd-parity solutions of the unperturbed disk.

In the near-degenerate situation, i.e., when the frequencies of two or more modes in the unperturbed disk are very similar, the perturbation theory needs to be modified [36]. Here, we discuss first the modifications for the case of two nearly degenerate modes by using a slightly different notation. The mode in the unperturbed disk with smaller radial mode number (and therefore higher Q factor) is called mode 1 and the other one is called mode 2. The azimuthal mode number of mode 1 is denoted by m, and that of mode 2 by $p < m$. By convention, we consider the frequency x_1 of mode 1 as the zeroth-order solution, i.e., $S_m(x_1) = 0$. The first-order correction $x_1\delta x$ can then be computed from the following set of equations [36]:

$$(s_1 - \delta x)a_1 = A^{e/o}_{mp} a_2, \tag{3}$$

$$(s_2 - \delta x)a_2 = A^{e/o}_{pm} a_1, \tag{4}$$

where a_1 (a_2) is the amplitude of mode 1 (2) and

$$s_1 = \frac{S_m(x_1)}{x_1(n^2-1)} - A^{e/o}_{mm}, \tag{5}$$

$$s_2 = \frac{S_p(x_1)}{x_1(n^2-1)} - A^{e/o}_{pp}. \tag{6}$$

The Fourier harmonics of the deformation function are given for even parity as

$$A^{e}_{pm} = \frac{\varepsilon_p}{\pi R}\int_0^\pi f(\phi)\cos(p\phi)\cos(m\phi)d\phi, \tag{7}$$

and for odd parity as

$$A^{o}_{pm} = \frac{\varepsilon_p}{\pi R}\int_0^\pi f(\phi)\sin(p\phi)\sin(m\phi)d\phi, \tag{8}$$

with $\varepsilon_p = 2$ if $p \neq 0$ and $\varepsilon_p = 1$ otherwise. Note that, in Eq. (6), it is assumed that $|S_p(x_1)| \ll |x_1|(n^2-1)$ which is satisfied for all interesting cases. This assumption is not mentioned in Ref. [36].

III. EFFECTIVE HAMILTONIAN FOR TWO NEARLY DEGENERATE MODES

In this section we rewrite the set of linear equations (3) and (4) as an eigenvalue problem of an effective Hamiltonian. We use the derivative [36]

$$\frac{\partial S_m}{\partial x}(x) = -(n^2-1) - \frac{S_m(x)}{x} - S_m(x)\left[S_m(x) + 2\frac{H'_m}{H_m}(x)\right]. \tag{9}$$

With the frequency x_2 of the second mode, $S_p(x_2) = 0$, we expand

$$S_p(x_1) = (n^2-1)(x_2 - x_1) \tag{10}$$

to first order of $x_2 - x_1$. Using Eq. (10) and $S_m(x_1) = 0$ we write the Eqs. (3) and (4) for the complex frequencies as the eigenvalue equation

$$\hat{H}\begin{pmatrix} a_1 \\ a_2 \end{pmatrix} = x\begin{pmatrix} a_1 \\ a_2 \end{pmatrix}, \tag{11}$$

with effective non-Hermitian Hamiltonian

$$\hat{H} = \begin{pmatrix} x_1 & 0 \\ 0 & x_2 \end{pmatrix} - x_1\begin{pmatrix} A^{e/o}_{mm} & A^{e/o}_{mp} \\ A^{e/o}_{pm} & A^{e/o}_{pp} \end{pmatrix}, \tag{12}$$

which describes the effect of a weak boundary deformation to first order in the formal perturbation parameter λ. Note that, for fixed parity, the coupling matrix elements $A^{e/o}_{mp}$ and $A^{e/o}_{pm}$ are equal as long as $m, p > 0$ [see Eqs. (7) and (8)] which is the case that we consider here. The matrix (12) is therefore complex symmetric.

The complex eigenvalues are the first-order frequencies $x = x_1(1 + \delta x)$, i.e.,

$$x_\pm = \frac{x_1 + x_2}{2} - x_1\frac{A^{e/o}_{mm} + A^{e/o}_{pp}}{2} \pm \sqrt{\frac{\left[x_1 - x_2 - x_1\left(A^{e/o}_{mm} - A^{e/o}_{pp}\right)\right]^2}{4} + x_1^2\left(A^{e/o}_{mp}\right)^2}. \tag{13}$$

In following we provide a necessary criterion for the applicability of the perturbation theory. In the expansion of $S_p(x_1)$ [Eq. (10)] the first order is assumed to be sufficient. This assumption, however, requires the second order of the expansion to be much smaller than the first order; i.e.

$$\left|\frac{1}{2}\frac{\partial^2 S_p}{\partial x^2}(x_2)(x_1 - x_2)^2\right| \ll \left|\frac{\partial S_p}{\partial x}(x_2)(x_1 - x_2)\right|. \tag{14}$$

By using the second derivative at the root $S_p(x_2) = 0$ [36],

$$\frac{\partial^2 S_p}{\partial x^2}(x_2) = (n^2-1)\left[\frac{1}{x_2} + 2\frac{H'_p}{H_p}(x_2)\right], \tag{15}$$

and Eq. (9) we can compare the first- and second-order terms and derive

$$|x_2 - x_1| \ll \frac{2|x_2|}{\left|1 + 2x_2\frac{H'_p}{H_p}(x_2)\right|} \tag{16}$$

as the criterion for the difference of the two initial wave numbers.

IV. SECOND ORDER EXCEPTIONAL POINT FOR GENERAL SMOOTH BOUNDARIES WITH FINE TUNING OF REFRACTIVE INDEX

In this section we restrict ourselves to boundary deformations that are sufficiently smooth such that the relevant Fourier integrals

$$\int_0^\pi f(\phi)\cos(q\phi)d\phi \tag{17}$$

are exactly zero or are so small that they can be ignored for $q \geqslant 2p$, where p is again the azimuthal mode number of mode 2. In this regime,

$$A^{e/o}_{mm} = A^{e/o}_{pp} = \frac{1}{\pi R}\int_0^\pi f(\phi)d\phi, \tag{18}$$

$$A^{e/o}_{mp} = \frac{1}{\pi R}\int_0^\pi f(\phi)\cos[(p-m)\phi]d\phi. \tag{19}$$

Moreover, as in Ref. [35], we adjust the refractive index such that $\mathrm{Re}(x_1) = \mathrm{Re}(x_2)$. Finally, we assume that $|\mathrm{Im}(x_1)| \ll |x_1|$, which is always fulfilled for whispering-gallery modes. The condition for the EP2, given by the vanishing of the radicand in Eq. (13), is then

$$4\left|A^{e/o}_{mp}\right| = \frac{1}{Q_2} - \frac{1}{Q_1}, \tag{20}$$

where $Q_j = -\mathrm{Re}(x_j)/[2\mathrm{Im}(x_j)]$ is the quality factor of mode j. Equation (20) shows that an extremely weak boundary deformation suffices to achieve an EP provided that the involved modes have high quality factors.

It is straightforward to show that the eigenvector at the EP is given by

$$\vec{v}_{\mathrm{EP}} = \begin{pmatrix} 1 \\ -i\ \mathrm{sgn}\, A^{e/o}_{mp} \end{pmatrix}, \tag{21}$$

where sgn is the sign function. This is the typical structure of the eigenvector $(1, \pm i)^T$ of a symmetric 2×2 matrix at an EP2 [38,39]. The phase lag of $\pi/2$ leads to a well-defined handedness, called chirality. The sign of the chirality is here given by $-\,\mathrm{sgn}\, A^{e/o}_{mp}$.

In the above approximation the Fourier coefficients in Eqs. (18) and (19) are the same for even- and odd-parity modes. This implies that both EP2s are located at the same parameter values, which means that, for fixed parameters, there is a pair of degenerate EP2s. One could take advantage of this degeneracy by introducing a further weak but now asymmetric deformation to generate an EP of order three or four.

An example

We consider the cavity with deformation function

$$f(\phi) = \varepsilon\frac{R}{16}[\cos(4\phi) - 1], \tag{22}$$

where ε is the dimensionless deformation parameter. This deformation function inserted into Eq. (2) is the first-order approximation in ε of the curve

$$x^2 + y^2(1 + \varepsilon x^2/R^2) = R^2 \tag{23}$$

studied in Ref. [35]. With the deformation function (22), Eqs. (12) and (19) imply the selection rule $|p - m| = 4$, i.e., only modes where the azimuthal mode numbers differ by ±4 are coupled within the first-order perturbation theory.

For the specific mode pair with $m = 22$ and $p = 18$ a short calculation shows that $A^{e/o}_{18,18} = A^{e/o}_{22,22} = -\varepsilon/16$ and $A^{e/o}_{18,22} = \varepsilon/32$. Inserting the latter intermediate result into Eq. (20) gives

$$|\varepsilon| = 8\left(\frac{1}{Q_2} - \frac{1}{Q_1}\right), \tag{24}$$

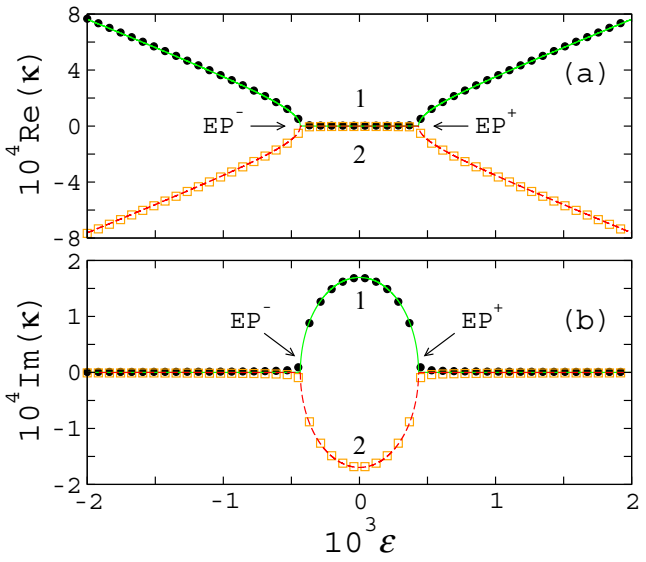

FIG. 1. (a) Real and (b) imaginary part of the frequency $\kappa \equiv x - \bar{x}$ relative to the mean frequency $\bar{x}$ of the two involved even-parity modes in the cavity (22). Marked are the two exceptional points of second order EP$^\pm$; mode 1 with $(m, l) = (22, 1)$ and mode 2 with $(p, \tilde{l}) = (18, 2)$ for $\varepsilon = 0$. Filled circles and open squares are BEM results and solid and dashed curves are the corresponding predictions of the perturbation theory [Eq. (13)]. The refractive index is $n = 2.105\,09$.

both for even and odd parity. Thus, in total there are four EPs: two for positive ε and two for negative ε. With the above value of $A^{e/o}_{18,22}$ it follows that the eigenvector from Eq. (21) is

$$\vec{v}_{\mathrm{EP}} = \begin{pmatrix} 1 \\ -i\ \mathrm{sgn}\,\varepsilon \end{pmatrix}. \tag{25}$$

Thus, the sign of the chirality of the EP is $-\,\mathrm{sgn}\,\varepsilon$. This implies that we get for each parity two EPs with opposite sign of the chirality, one for negative and one for positive ε; see Eqs. (24) and (25). Note that the analytical predictions in Eqs. (24) and (25) are not provided by the resonance-assisted tunneling approach in Ref. [35].

For the two modes considered with $(m, l) = (22, 1)$ and $(p, \tilde{l}) = (18, 2)$ we can tune the real part of their frequency on resonance by choosing $n = 2.105\,09$. With $x_1 = 12.499\,64 - i1.159\,48\times10^{-7}$ and $x_2 = 12.499\,64 - i3.393\,93\times10^{-4}$ we get from Eq. (24) $|\varepsilon| = 0.000\,43$ and for both EPs $x_\pm = 12.499\,30 - 1.697\,54\times10^{-4}$ in very good agreement with Ref. [35]. Figure 1 demonstrates the agreement with numerical results for even-parity modes using the boundary element method (BEM) [40]. Clearly visible is the existence of two EPs located at $\varepsilon \approx \pm0.000\,45$. Note that the criterion (16) is fulfilled because $3.4\times10^{-4} \ll 1.136$.

Figure 2 shows the Poynting vector $\vec{J}$ for both EPs. The chirality of the EPs shows up here by the local vortex structure of $\vec{J}$, which we call local chirality [35]. The opposite circulation of the vortex in Figs. 2(a) and 2(b) demonstrates that both EPs have a different sign of the chirality consistent with the prediction in Eq. (25).

The mode patterns at the EPs and, for comparison, in the unperturbed cavity are shown in Fig. 3. The irregular nodal

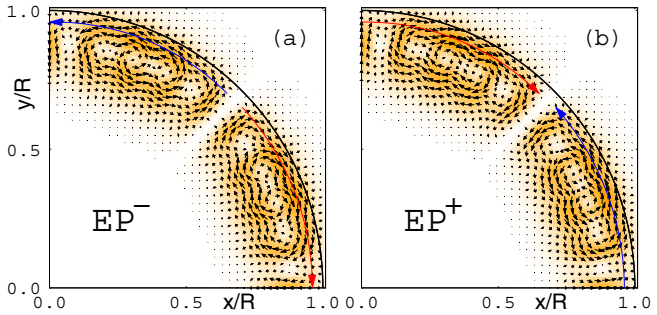

FIG. 2. Numerically computed Poynting vector $\vec{J} \propto \mathrm{Im}\,(\psi^* \vec{\nabla} \psi)$ of the mode at (a) EP$^-$ and (b) EP$^+$ in Fig. 1. Long arrows mark the dominant stream of the Poynting vector in the vicinity of the cavity boundary (quarter-circular curve). Shading represents $|\vec{J}|$ normalized to be zero at the minimum (white) and unity at the maximum (gray or yellow).

pattern and the strongly reduced interference pattern in the radial direction is a clear signature of the structure in Eq. (25) and is related to an abnormal localization in ray-dynamical phase space, as discussed in Ref. [35].

V. SECOND-ORDER EXCEPTIONAL POINT FOR SPECIALLY DESIGNED BOUNDARIES

This section shows that, for a given nearly degenerate pair of modes with azimuthal mode numbers m and $p < m$, we can design a boundary such that an EP can be generated without the need to fine tune the refractive index. We consider the family of cavities

$$f(\phi) = \frac{\varepsilon}{2} R \cos\left[(m-p)\phi\right] + 2\sigma R \cos(2m\phi), \tag{26}$$

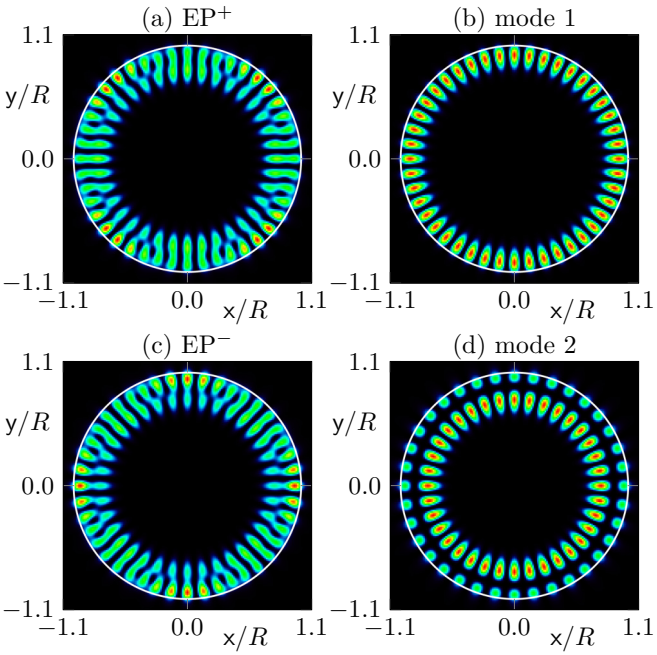

FIG. 3. Intensities $|\psi|^2$ of modes calculated by the BEM and marked by the same labels as in Fig. 1. (a) EP$^+$, (b) mode 1 with $(m, l) = (22, 1)$, (c) EP$^-$, and (d) mode 2 with $(p, \tilde{l}) = (18, 2)$.

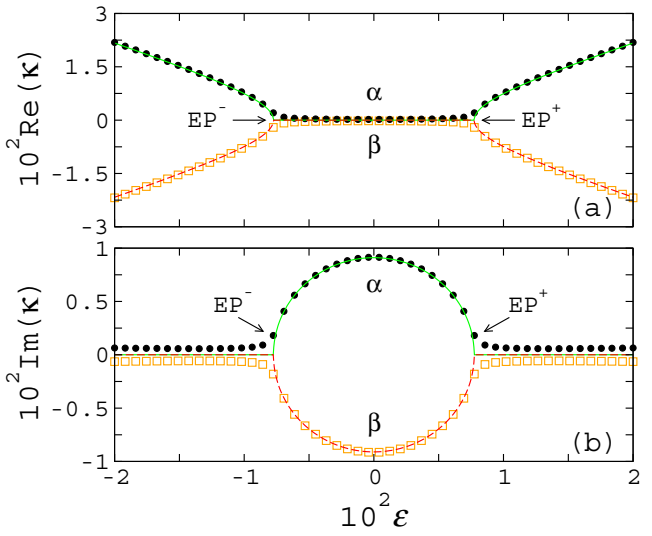

FIG. 4. (a) Real and (b) imaginary part of the frequency $\kappa \equiv x - \overline{x}$ relative to the mean frequency $\overline{x}$ of the two modes involved in the cavity (26) with $\sigma = 1.646\times10^{-3}$ and refractive index $n = 3.3$. Filled circles and open squares are BEM results for modes $(m, l) = (12, 1)$ and $(p, \tilde{l}) = (6, 3)$ (α and β when $\varepsilon = 0$). Solid and dashed curves are the predictions of the perturbation theory [Eq. (13)].

with two dimensionless deformation parameters ε and σ. It is important to realize that in the following we do not ignore any Fourier integrals (17). Excluding the special case $m \neq 3p$ we get $A^{e/o}_{mp} = \varepsilon/4$, $A^{e/o}_{pp} = 0$, and $A^{e/o}_{mm} = \pm\sigma$, where the $+$ $(-)$ is for even (odd) parity. Stipulating again $|\mathrm{Im}(x_1)| \ll |x_1|$, it is straightforward to show that the real part of $x_1 - x_2$ in the square root in Eq. (13) can be canceled by the term $x_1(A^{e/o}_{mm} - A^{e/o}_{pp})$ provided that

$$\sigma = \pm \frac{\mathrm{Re}(x_1 - x_2)}{\mathrm{Re}(x_1)}. \tag{27}$$

For even-parity modes we have to choose the $+$ sign and for the odd-parity modes the $-$ sign. To generate the EP, one then has to tune ε analogous to Eq. (24):

$$|\varepsilon| = \frac{1}{Q_2} - \frac{1}{Q_1}. \tag{28}$$

Both parameters σ and ε are small numbers provided that the modes are nearly degenerate and have high quality factors. Hence, the boundary deformation is expected to be very weak. A short calculation shows that the eigenvector at the EPs is given by Eq. (25). Hence, the sign of the chirality of the EP is again $-\,\mathrm{sgn}\,\varepsilon$.

To illustrate the theory we choose as an example the modes $(m, l) = (12, 1)$ and $(p, \tilde{l}) = (6, 3)$ in a cavity with refractive index $n = 3.3$ (e.g., GaAs) which is considerably different from the fine-tuned refractive index (=3.631 75) following the scheme in Sec. IV. In our new scheme we get from Eqs. (27) and (28) the values $\sigma = 1.646\times10^{-3}$ and $|\varepsilon| = 7.7\times10^{-3}$. Figure 4 confirms with BEM results that, with these parameter values, two EPs are indeed located. Figure 5 proves that the sign of the chirality of the two EPs is opposite, in accordance with Eq. (25). The modes at the EPs and the modes at $\varepsilon = 0$ are

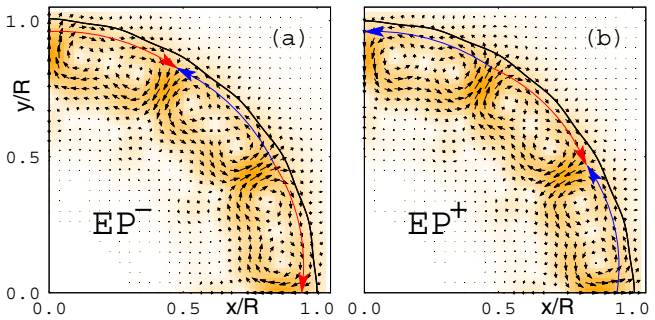

FIG. 5. Numerically computed Poynting vector $\vec{J}$ of the mode at the (a) EP$^-$ and (b) EP$^+$ in Fig. 4. Long arrows mark the dominant stream of the Poynting vector in the vicinity of the cavity boundary (corrugated quarter-circular curve). Shading represents $|\vec{J}|$ normalized to be zero at the minimum (white) and unity at the maximum (gray or yellow).

depicted in Fig. 6. Note also in this example that the criterion (16) is fulfilled because $1.98\times10^{-2} \ll 1.8148$.

VI. THIRD-ORDER EXCEPTIONAL POINT FOR SPECIALLY DESIGNED BOUNDARIES

In this section we apply the perturbative scheme to the case of three involved modes which are nearly degenerate in the circular cavity. The azimuthal mode numbers of modes 1 to 3 are ordered according to $m > p > q$. In the same spirit as in Eq. (11) the complex frequencies of the deformed cavity can be obtained by means of the perturbation theory from the eigenvalue equation of an effective non-Hermitian

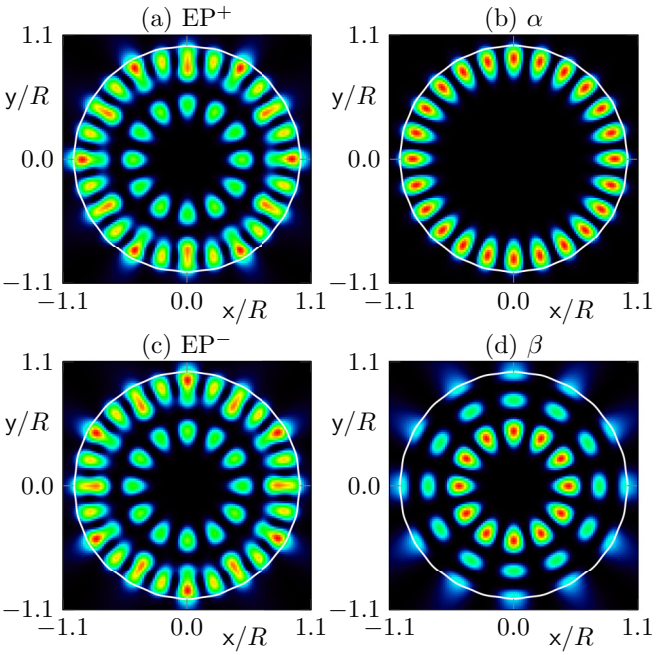

FIG. 6. Intensities $|\psi|^2$ of modes calculated with the BEM and marked by the same labels as in Fig. 4; $\sigma = 1.646\times10^{-3}$. (a) EP$^+$, (b) mode α with $(m, l) = (12, 1)$, (c) EP$^-$, and (d) mode β with $(p, \tilde{l}) = (6, 3)$.

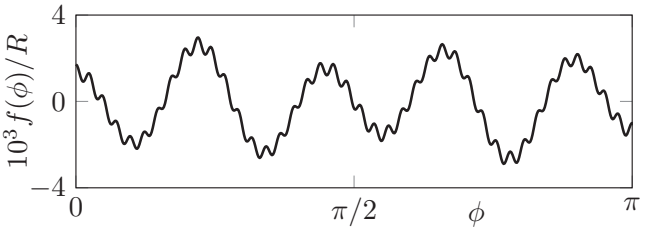

FIG. 7. Boundary deformation function $f(\phi)$ corresponding to the EP3 configuration (36). Only the interval $\phi \in [0, \pi]$ is shown. The remaining part $[-\pi, 0]$ is given by symmetry.

Hamiltonian

$$\hat{H} = \begin{pmatrix} x_1 & 0 & 0 \\ 0 & x_2 & 0 \\ 0 & 0 & x_3 \end{pmatrix} - x_1 \begin{pmatrix} A^{e/o}_{mm} & A^{e/o}_{mp} & A^{e/o}_{mq} \\ A^{e/o}_{pm} & A^{e/o}_{pp} & A^{e/o}_{pq} \\ A^{e/o}_{qm} & A^{e/o}_{qp} & A^{e/o}_{qq} \end{pmatrix}. \quad (29)$$

The eigenvectors of $\hat{H}$ correspond to the amplitudes of the modes. A fine tuning of the refractive index might provide equal values of $\mathrm{Re}(x)$ for two modes in the circular cavity. However, it is unlikely that all three nearly degenerate modes can be arranged by a refractive index variation such that $\mathrm{Re}(x_1) = \mathrm{Re}(x_2) = \mathrm{Re}(x_3)$. Thus, in order to achieve a EP3 the slight differences in $\mathrm{Re}(x)$ also need to be compensated by the boundary deformation. In the following, we therefore consider in analogy to Eq. (26) the family of cavities described by

$$\begin{aligned} \frac{f(\phi)}{R} = {} & 2\epsilon_1 \cos[(m-p)\phi] + 2\epsilon_2 \cos[(p-q)\phi] \\ & + 2\epsilon_3 \cos[(m-q)\phi] \\ & + 2\sigma_p \cos(2p\phi) + 2\sigma_q \cos(2q\phi). \end{aligned} \quad (30)$$

Moreover, we assume that all cosine terms have different periods; i.e., $m - p \neq p - q \neq 2p \neq \cdots$. Thus, ϵ_1, ϵ_2, ϵ_3, σ_p, and σ_q represent five independent parameters which are in general necessary for tuning a symmetric matrix to a EP3. For the considered boundary deformation, the Hamiltonian (29) can be written for the even-parity modes as

$$\hat{H} = -x_1 \begin{pmatrix} -1 & \epsilon_1 & \epsilon_3 \\ \epsilon_1 & \sigma_p - \dfrac{x_2}{x_1} & \epsilon_2 \\ \epsilon_3 & \epsilon_2 & \sigma_q - \dfrac{x_3}{x_1} \end{pmatrix}. \quad (31)$$

For odd parity, σ_p (σ_q) needs to be replaced by $-\sigma_p$ ($-\sigma_q$).

In the following we consider an example of three quasidegenerate modes in a circular cavity with refractive index $n = 1.5$ (e.g., PMMA), as mentioned in Ref. [36]. The unperturbed frequencies and mode numbers (azimuthal, radial) are

$$x_1 = 34.311\,00 - i2.220\,63\times10^{-6} \quad (46, 1), \quad (32)$$

$$x_2 = 34.316\,74 - i1.981\,69\times10^{-3} \quad (41, 2), \quad (33)$$

$$x_3 = 34.311\,72 - i6.407\,80\times10^{-2} \quad (37, 3). \quad (34)$$

In contrast with the case of EP2s we cannot derive analytical formulas for the location of the EP3 in parameter space. Thus,

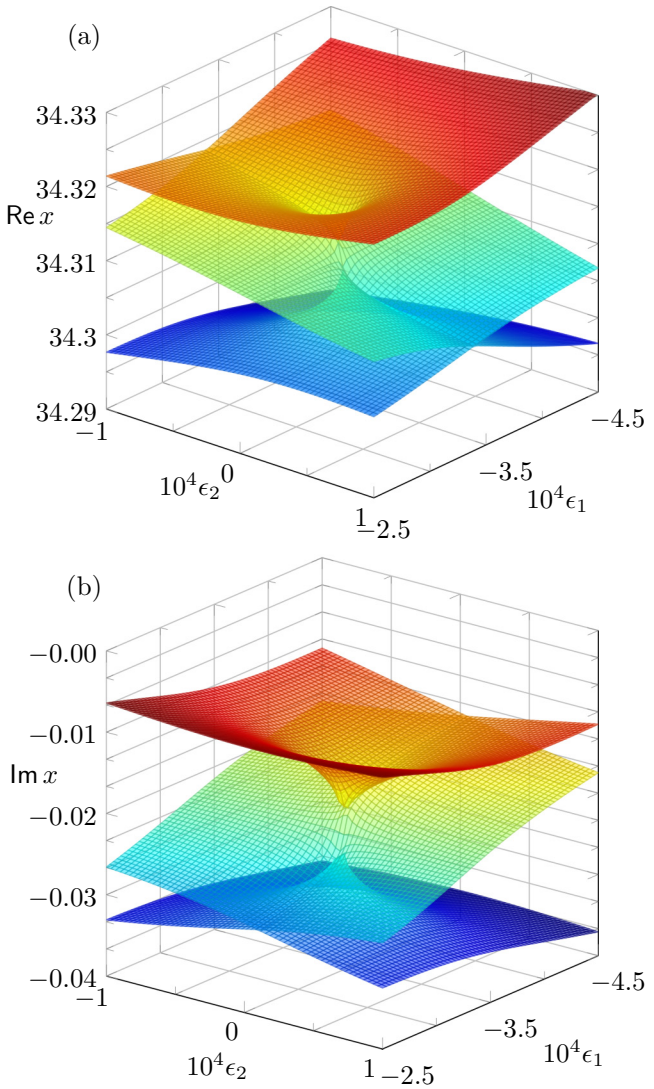

FIG. 8. (a) Real and (b) imaginary part of the dimensionless frequencies x obtained from the eigenvalues of $\hat{H}$ [see Eq. (31)] around the EP3. The (dimensionless) deformation parameters varied are ϵ_1 and ϵ_2. Note that the parameters are scaled with 10^4. The color maps range from blue to red according to the z axes.

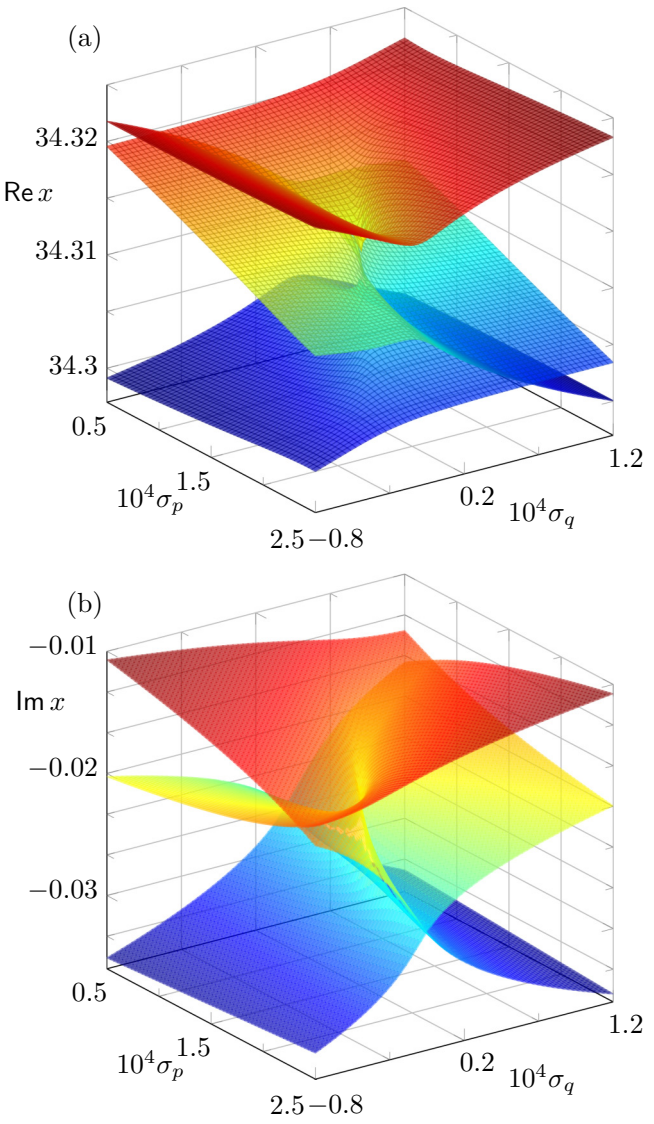

FIG. 9. (a) Real and (b) imaginary part of the dimensionless frequencies x obtained from the eigenvalues of $\hat{H}$ [see Eq. (31)] around the EP3. The (dimensionless) deformation parameters varied are σ_p and σ_q (scaled with 10^4). The color maps range from blue to red according to the z axes.

we numerically determine a particular deformation resulting in a EP3 for the even-parity modes from the Hamiltonian (31) as follows: For a given set of deformation parameters we calculate the eigenvectors $\vec{v}_i$ of the Hamiltonian (31) and define the auxiliary function

$$g = \sum_{i \neq j} (|\vec{v}_i^{\,*} \cdot \vec{v}_j| - 1)^2. \tag{35}$$

At a EP3 this function has a local minimum with $g = 0$. By using a downhill simplex method with a randomly chosen small initial deformation we can obtain such a local minimum and thus a EP3. Note that one may needs to re-initialize the minimum search with a different initial deformation if the auxiliary function g is finite at the determined local minimum. As an example among others we obtain the deformation parameters of the EP3:

$$\epsilon_{1,\mathrm{EP}} = -0.000\,331\,738\,548\,465, \tag{36a}$$
$$\epsilon_{2,\mathrm{EP}} = 0.000\,007\,162\,344\,726, \tag{36b}$$
$$\epsilon_{3,\mathrm{EP}} = 0.001\,008\,753\,672\,052, \tag{36c}$$
$$\sigma_{p,\mathrm{EP}} = 0.000\,156\,738\,979\,431, \tag{36d}$$
$$\sigma_{q,\mathrm{EP}} = 0.000\,015\,861\,604\,093. \tag{36e}$$

The corresponding deformation function is shown in Fig. 7.

The numerically determined normalized eigenvector at the EP3 is

$$\vec{v}_{\mathrm{EP3}} \approx \begin{pmatrix} 0.7071 \\ 0.0036 + 0.4017i \\ -0.0025 + 0.5819i \end{pmatrix}. \tag{37}$$

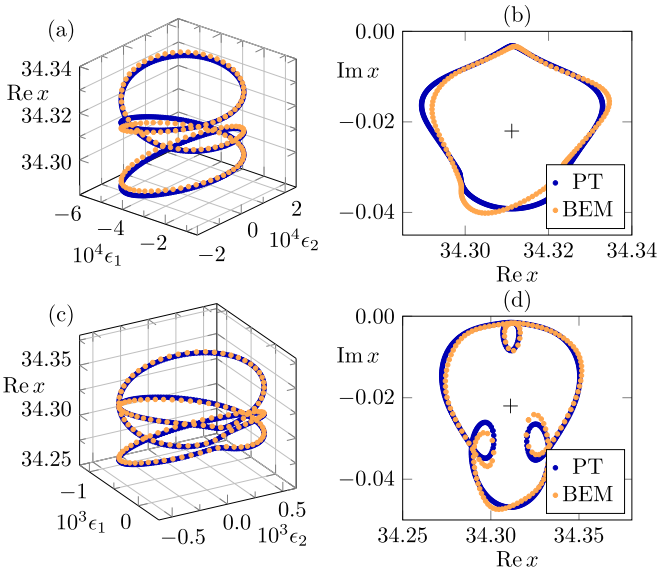

FIG. 10. (a), (c) Real part of the frequencies along a parameter path in ϵ_1-ϵ_2 plane (dimensionless) which encircles the EP3 three times with radius (a) $\rho = 2\times10^{-4}$ and (c) $\rho = 6\times10^{-4}$. In panel (b) and (d), the corresponding rotations of the dimensionless frequencies x are shown in the complex plane. Results from perturbation theory (PT, dark or blue curve) are compared with BEM calculations (light or orange dots). In panels (b) and (d) the frequency at the EP3 is marked with a plus sign.

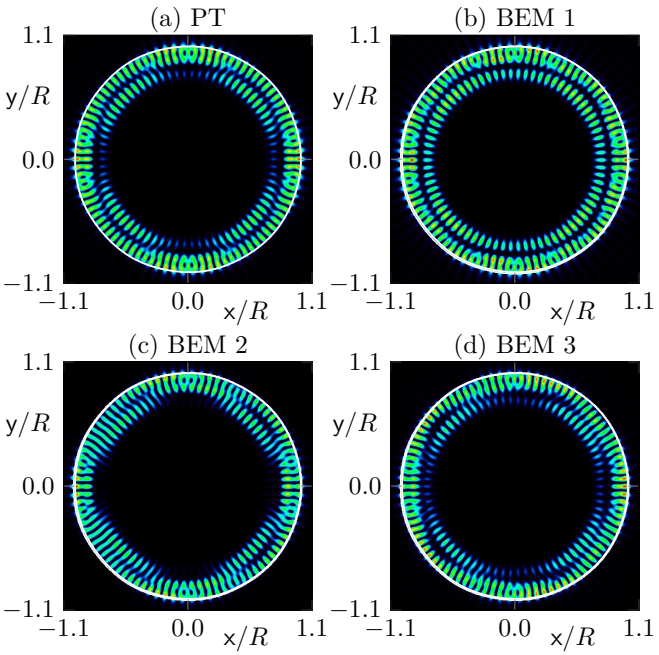

FIG. 11. Intensity patterns $|\psi|^2$ of the modes at the EP3 of the Hamiltonian $\hat{H}$ [configuration (36)]. The prediction of the perturbation theory in panel (a) is compared with the three nearly degenerate modes obtained by the BEM in panels (b)–(d).

In Figs. 8 and 9 the frequencies in the deformed cavity are shown in ϵ_1-ϵ_2 and σ_p-σ_q parameter plane, respectively. At the configuration (36) all three complex frequencies indeed coalesce, which marks the EP3. From Cardano's formulas it follows that the frequency at the EP3 is given by

$$x_{\mathrm{EP3}} = \frac{x_1 + x_2 + x_3}{3} - \frac{x_1(\sigma_p + \sigma_q)}{3}. \tag{38}$$

In the vicinity of the EP3 a characteristic cubic root topology of the frequencies is obtained. Depending on the specific choice of deformation parameters to be varied, the appearance of the frequency surfaces might be different, as can be seen by comparing Figs. 8 and 9. However, the characteristics of the cubic-root topology can be seen in both figures. As one continuously changes the deformation parameters along a closed loop encircling the EP3, the complex frequencies (and the corresponding modes) interchange simultaneously. In particular, the EP3 needs to be encircled three times along a closed loop in parameter space to get closed frequency trajectories in the complex plane [21]. Such a threefold encircling in ϵ_1-ϵ_2 parameter space is shown in Fig. 10 for two different radii $\rho = [(\epsilon_1 - \epsilon_{1,\mathrm{EP}})^2 + (\epsilon_2 - \epsilon_{2,\mathrm{EP}})^2]^{1/2}$. For a relatively small radius $\rho = 2\times10^{-4}$, the real parts of the frequencies [Fig. 10(a)] follow the expectation from the cubic root topology in Fig. 8(a). During one encircling in parameter space all three frequencies perform a simple rotation around the EP3 in the complex x plane [Fig. 10(b)]. If the EP3 is encircled three times with a larger radius $\rho = 6\times10^{-4}$ the loops of $\mathrm{Re}(x)$ have more than two intersections [Fig. 10(c)]. Simultaneously, the rotations of the frequency in complex x plane show additional loops related to EP2s which are now also encircled in parameter space. Additionally, Fig. 10 demonstrates a very good agreement between the perturbation theory and numerical BEM calculation in the vicinity of the EP3. However, very close to the EP3, slight deviations between perturbation theory and BEM occur because the determined parameter (36) does not correspond exactly to the EP3 in BEM calculations. Thus, due to the very high sensitivity of the frequencies at the EP3, one can distinguish three modes for the configuration (36) with BEM. The intensity patterns of these modes, however, look similar to the one predicted by perturbation theory; see Fig. 11. This visual similarity can be confirmed numerically by the normalized overlap

$$S[\psi_i, \psi_j] = \frac{|\int_{\mathrm{cavity}} \psi_i^* \psi_j d^2r|}{\sqrt{\int_{\mathrm{cavity}} |\psi_i|^2 d^2r \int_{\mathrm{cavity}} |\psi_j|^2 d^2r}} \tag{39}$$

of two modes. For all three BEM modes in Figs. 11(b)–11(d) the overlap to the predicted mode [Fig. 11(a)] is $S[\psi_{\mathrm{PT}}, \psi_j] \approx 0.96$. Additionally, the pairwise overlap of the BEM modes is $S[\psi_i, \psi_j] \approx 0.9$ reflecting the strong pairwise nonorthogonality of the three modes close to a EP3.

Moreover, it is known (see Refs. [22,41]) that, at an EP3, the mode becomes self-orthogonal in the sense $S[\psi_i^*, \psi_i] \to 0$. For the eigenvector (37) we find $S[\psi_i^*, \psi_i] \approx 2\times10^{-5}$. Note that $S[\psi_i, \psi_i]$ is always unity. Despite the BEM not being exactly at the EP3, notable remnants of the self-orthogonality can be obtained from the BEM modes [Figs. 11(b)–11(d)] as $S[\psi_i^*, \psi_i] \approx 0.2$ which is still significantly below one.

Furthermore, it is mentioned that the nodal lines in the intensity patterns are blurred locally, which is again a signature of the local chirality of the modes.

VII. CONCLUSION

In the paper we presented a perturbative approach for exceptional points in weakly deformed microdisks. We derived an effective non-Hermitian Hamiltonian which describes the coupling of optical modes with different angular momentum. If compared with the resonance-assisted tunneling approach in Ref. [35], the advantage of the proposed perturbative scheme is fourfold: (i) explicit analytical formulas [Eqs. (20) and (24)] are derived for the critical boundary deformation at which the EP takes place, (ii) the sign of the chirality of the EP can be predicted, (iii) our approach can find EPs in weakly deformed cavities without the need to fine tune the refractive index, and (iv) the approach can be extended to higher-order EPs.

In this work we demonstrated the feasibility of our theory not only for second-order EPs but also for third-order EPs which are hard to find otherwise in deformed microdisk cavities. In principle, our theory allows us to access even higher-order EPs in such systems which might be very useful for sensing applications.

ACKNOWLEDGMENT

We would like to thank L. Ge and Y.-F. Xiao for discussions. This work was supported by the DFG (Project No. WI1986/7-1).

[1] T. Kato, *Perturbation Theory for Linear Operators* (Springer, New York, 1966).
[2] W. D. Heiss, Phys. Rev. E **61**, 929 (2000).
[3] M. V. Berry, Czech. J. Phys. B **54**, 1039 (2004).
[4] C. Dembowski, H.-D. Gräf, H. L. Harney, A. Heine, W. D. Heiss, H. Rehfeld, and A. Richter, Phys. Rev. Lett. **86**, 787 (2001).
[5] C. Dembowski, B. Dietz, H.-D. Gräf, H. L. Harney, A. Heine, W. D. Heiss, and A. Richter, Phys. Rev. E **69**, 056216 (2004).
[6] S.-B. Lee, J. Yang, S. Moon, S.-Y. Lee, J.-B. Shim, S. W. Kim, J.-H. Lee, and K. An, Phys. Rev. Lett. **103**, 134101 (2009).
[7] J. Zhu, Ş. K. Özdemir, L. He, and L. Yang, Opt. Express **18**, 23535 (2010).
[8] B. Peng, Ş. K. Özdemir, F. Lei, F. Monfi, M. Gianfreda, G. L. Long, S. Fan, F. Nori, C. M. Bender, and L. Yang, Nat. Phys. **10**, 394 (2014).
[9] B. Peng, Ş. K. Özdemir, M. Liertzer, W. Chen, J. Kramer, H. Yilmaz, J. Wiersig, S. Rotter, and L. Yang, Proc. Natl. Acad. Sci. USA **113**, 6845 (2016).
[10] Y. Choi, S. Kang, S. Lim, W. Kim, J.-R. Kim, J.-H. Lee, and K. An, Phys. Rev. Lett. **104**, 153601 (2010).
[11] T. Gao, E. Estrecho, K. Y. Bliokh, T. C. H. Liev, M. D. Fraser, S. Brodbeck, M. Kamp, C. Schneider, S. Höfling, Y. Yamamoto *et al.*, Nature (London) **526**, 554 (2015).
[12] Y. Shin, H. Kwak, S. Moon, S.-B. Lee, J. Yang, and K. An, Sci. Rep. **6**, 38826 (2016).
[13] J. Wiersig, Phys. Rev. Lett. **112**, 203901 (2014).
[14] W. Chen, Ş. K. Özdemir, G. Zhao, J. Wiersig, and L. Yang, Nature (London) **548**, 192 (2017).
[15] P. Miao, Z. Zhang, J. Sun, W. Walasik, S. Longhi, N. M. Litchinitser, and L. Feng, Science **353**, 464 (2016).
[16] S. Richter, T. Michalsky, C. Sturm, B. Rosenow, M. Grundmann, and R. Schmidt-Grund, Phys. Rev. A **95**, 023836 (2017).
[17] H. Xu, D. Mason, L. Jiang, and J. G. E. Harris, Nature (London) **537**, 80 (2016).
[18] J. Doppler, A. A. Mailybaev, J. Böhm, U. Kuhl, A. Girschik, F. Libisch, T. J. Milburn, P. Rabl, N. Moiseyev, and S. Rotter, Nature (London) **537**, 76 (2016).
[19] K. Ding, G. Ma, M. Xiao, Z. Q. Zhang, and C. T. Chan, Phys. Rev. X **6**, 021007 (2016).
[20] H. Hodaei, A. Hassan, S. Wittek, H. Carcia-Cracia, R. El-Ganainy, D. Christodoulides, and M. Khajavikhan, Nature (London) **548**, 187 (2017).
[21] G. Demange and E.-M. Graefe, J. Phys. A: Math. Theor. **45**, 025303 (2012).
[22] W. D. Heiss, J. Phys. A: Math. Theor. **41**, 244010 (2008).
[23] Q. Zhong, D. N. Christodoulides, M. Khajavikhan, K. G. Makris, and R. El-Ganainy, Phys. Rev. A **97**, 020105(R) (2018).
[24] P. Michler, A. Kiraz, C. Becher, W. V. Schoenfeld, P. M. Petroff, L. Zhang, E. Hu, and A. Imamoğlu, Science **290**, 2282 (2000).
[25] J. Wiersig, C. Gies, F. Jahnke, M. Aßmann, T. Berstermann, M. Bayer, C. Kistner, S. Reitzenstein, C. Schneider, S. Höfling *et al.*, Nature (London) **460**, 245 (2009).
[26] N. Akopian, N. H. Lindner, E. Poem, Y. Berlatzky, J. Avron, D. Gershoni, B. D. Gerardot, and P. M. Petroff, Phys. Rev. Lett. **96**, 130501 (2006).
[27] H. Cao and J. Wiersig, Rev. Mod. Phys. **87**, 61 (2015).
[28] J. U. Nöckel and A. D. Stone, Nature (London) **385**, 45 (1997).
[29] C. Gmachl, F. Capasso, E. E. Narimanov, J. U. Nöckel, A. D. Stone, J. Faist, D. L. Sivco, and A. Y. Cho, Science **280**, 1556 (1998).
[30] J. Wiersig and M. Hentschel, Phys. Rev. Lett. **100**, 033901 (2008).
[31] Q. J. Wang, C. Yan, N. Yu, J. Unterhinninghofen, J. Wiersig, C. Pflügl, L. Diehl, T. Edamura, M. Yamanishi, H. Kan *et al.*, Proc. Natl. Acad. Sci. USA **107**, 22407 (2010).
[32] X.-F. Jiang, Y.-F. Xiao, C.-L. Zou, L. He, C.-H. Dong, B.-B. Li, Y. Li, F.-W. Sun, L. Yang, and Q. Gong, Adv. Mater. **24**, OP260 (2012).
[33] A. Schlehahn, F. Albert, C. Schneider, S. Höfling, S. Reitzenstein, J. Wiersig, and M. Kamp, Opt. Express **21**, 15951 (2013).

[34] X. Jiang, L. Shao, S.-X. Zhang, X. Yi, J. Wiersig, L. Wang, Q. Gong, M. Loncar, L. Yang, and Y.-F. Xiao, Science **358**, 344 (2017).
[35] C.-H. Yi, J. Kullig, and J. Wiersig, Phys. Rev. Lett. **120**, 093902 (2018).
[36] R. Dubertrand, E. Bogomolny, N. Djellali, M. Lebental, and C. Schmit, Phys. Rev. A **77**, 013804 (2008).
[37] J. Kullig and J. Wiersig, Phys. Rev. A **94**, 043850 (2016).
[38] W. D. Heiss and H. L. Harney, Eur. Phys. J. D **17**, 149 (2001).
[39] C. Dembowski, B. Dietz, H.-D. Gräf, H. L. Harney, A. Heine, W. D. Heiss, and A. Richter, Phys. Rev. Lett. **90**, 034101 (2003).
[40] J. Wiersig, J. Opt. A **5**, 53 (2003).
[41] N. Moiseyev, *Non-Hermitian Quantum Mechanics* (Cambridge University Press, Cambridge, 2011).